

# Distinguished trajectories in time dependent vector fields

J. A. Jiménez Madrid, Ana M. Mancho  
Instituto de Ciencias Matemáticas (CSIC-UAM-UC3M-UCM),  
Serrano 121, 28006 Madrid (Spain)

December 11, 2021

## Abstract

We introduce a new definition of distinguished trajectory that generalises the concept of fixed point and periodic orbit to aperiodic dynamical systems. This new definition is valid to identify distinguished trajectories with hyperbolic and non hyperbolic type of stability. The definition is numerically implemented and the procedure consist of determining a path of *limit coordinates*. It has been successfully applied to known examples of distinguished trajectories. In the context of highly aperiodic realistic flows our definition characterizes *distinguished trajectories* in finite time intervals, and states that beyond those times trajectories are not longer *distinguished*.

Corresponding author: Ana M. Mancho, Instituto de Ciencias Matemáticas,  
Consejo Superior de Investigaciones Científicas, Serrano 121, 28006, Madrid. e-  
mail: A.M.Mancho@imaff.cfmac.csic.es. Phone: +34 91 5616800 ext 2408. Fax:  
+34 91 5854894.

This paper is an attempt to generalize the concept of fixed point and periodic orbit to time dependent aperiodic dynamical systems. Fixed points and periodic orbits are a keystone to describe the solutions of autonomous and time periodic dynamical systems, as the stable and unstable manifolds of these hyperbolic objects are on the basis of the geometrical template organizing the flow in the dynamical system. The mathematical theory of aperiodic dynamical systems is far from being complete. In this context, this work deals with a general definition that encloses the concepts of fixed point and periodic orbit, but that if it is applied to finite time and non periodic dynamical systems is able to identify special trajectories that play a particular role in the geometrical organization of the flow.

## 1 Introduction

The theory of dynamical systems has provided in recent years a good framework to describe transport in fluid flows. Since the seminal works by Aref [1] on chaotic advection many progress has been done both on theory and applications on this topic. Dynamical systems techniques were first applied to Lagrangian transport in the context of two-dimensional, time-periodic flows [2] and stationary 3D flows as the ABC flow [3]. More recently these techniques have been extended to describe aperiodic flows [4, 7, 8] and finite time dependent flows, as those rising in geophysical applications [11, 12]. However, the mathematical theory for both aperiodic time dependent flows and finite time aperiodic flows is far from being completely developed.

In stationary flows the idea of *fixed point* is a keystone to describe geometrically the solutions of dynamical systems. Fixed points may be classified as hyperbolic or non-hyperbolic depending on their stability properties which

describe the local behaviour around them. Stable and unstable manifolds of hyperbolic fixed points organize the flow in the global space, beyond the local region close to the fixed points [5, 6]. These manifolds are defined respectively by the set of initial conditions that in plus or minus infinite time infinitely approach the fixed points. As they are made of trajectories they are barriers to transport as particles cannot cross them without violating the unicity of the solution. They are useful because they allow qualitative predictions for the evolution of sets of initial conditions avoiding an explicit integration of initial conditions on the whole domain. Hyperbolic fixed points and their stable and unstable manifolds are on the basis of the geometrical template organizing the flow in autonomous dynamical systems.

The concept of fixed point is extended to time periodic flows by means of the Poincaré map, as periodic orbits with  $T$  period become fixed points on the Poincaré map which restricts a continuous orbit to its values taken in  $T$  intervals. For hyperbolic periodic orbits there exist also stable and unstable manifolds organizing the flow on the whole domain. Again they are respectively defined by the set of initial conditions that in plus or minus infinite time infinitely approach the periodic orbit.

Aperiodic flows are still poorly understood as theory which is well established in autonomous or periodic flows is not directly applicable to them. For instance there exists efforts in the mathematical community to extend the well known concept of 'bifurcation' in stationary flows to non-autonomous systems [9, 10]. To gain insight on the geometrical structure of aperiodic flows concepts such as Lyapunov exponents are used, however these are defined strictly on infinite time systems. Real flows present in geophysics or oceanography are not infinite time and to describe them, finite time versions of the definition of Lyapunov exponents such as Finite Size Lyapunov Exponents (FSLE) [14] and Finite Time Lyapunov Exponents (FTLE) [15, 16] are introduced. Special tra-

jectories, such as detachment and reattachment points [19], are recognized in highly aperiodic or turbulent flows. In particular these separation trajectories are identified on the boundaries of simplified ocean models [21] and also in technological applications in airfoil design [20]. Recent articles by Ide *et al* and Ju *et al* [17, 18] refer to these special trajectories introducing the concept of *Distinguished Hyperbolic Trajectory* (DHT) which stands not only for trajectories on the boundaries but also for special trajectories in the interior of the flow. DHT are hyperbolic trajectories that like hyperbolic fixed points and periodic orbits have stable and unstable manifolds that provide a geometrical template organizing the flow. This generalization is an important step-forwards in the study of aperiodic flows, as it is a powerful tool to describe transport in realistic oceanographic flows [11, 12, 13, 27]. Distinguished hyperbolic trajectories as defined in [17, 18] are computed from hyperbolic instantaneous stagnation points (ISPs) by means of an iterative procedure. If instantaneous stagnation points bifurcate and do not persist at all times the technique developed in [17, 18] cannot be applied, and then many open questions are left unanswered as distinguished hyperbolic trajectories are trajectories, and as trajectories exist at all times. In fact Ref. [11] provides examples of vector fields with exact distinguished hyperbolic trajectories that exist at time intervals without hyperbolic ISP. Refs. [11, 12] discuss the impossibility of this technique to track DHTs after ISPs bifurcations and as consequence the difficulties to establish whether DHTs obtained at different times are part of the same trajectory or not.

In this article, following ideas discussed in [11, 17, 18], we propose a new definition of *Distinguished Trajectory* (DT) which generalizes the concepts of fixed point and periodic orbit to aperiodic flows. We have taken the liberty to name them *Distinguished* as in [17, 18, 11] since although as explained below both definitions are not strictly equivalent, it is found that they are approaching the same trajectories. As an advantage over the method proposed in [17, 18] we

remark that ours may be computed without the presence of hyperbolic instantaneous stagnation points. Our definition does not depend on the dimension  $n$  of the vector field and is valid both for hyperbolic and non-hyperbolic type of stabilities. Non-hyperbolic DT have not been studied in [17, 18], and in this sense our definition is broader than the proposed there. In particular, we will show that exact non-hyperbolic periodic orbits fall within the category of distinguished trajectories. This type of trajectories might be of special interest for their applications in oceanography as they are related to eddies or vortices. Eddies are a well studied ocean structure [28]. Frequently they are long lived, and water trapped inside can maintain its biogeochemical properties for long time, being transported with the vortex. In steady horizontal velocity fields, the presence of closed streamlines around them is the mathematical reason for the isolation of the vortex core from the exterior fluid. In two dimensional, incompressible, time-periodic velocity fields the KAM tori encloses *the core*, a region of bounded fluid particles motions that does not mix up with the surrounding region [4]. But how to define an eddy from the Lagrangian point of view in aperiodic flows? This is still an open question [27, 29] for which we will discuss new insights provided by the definitions given in this article.

The structure of the paper is as follows. Section 2 introduces the definition of distinguished trajectory and explains its motivation in the context of 1D examples. Section 3 explains the algorithm used to verify our definition of distinguished trajectory over the periodically forced Duffing equation. Details over technical issues raised implementing the definition are given. Section 4 informs about the results obtained in several other 2D examples, both periodic and non periodic, hyperbolic and non hyperbolic. Section 5 discusses the results on realistic flows and attention is paid to open questions on distinguished trajectories such as those mentioned above and pointed out in Refs. [12, 11]. Finally section 6 presents the Conclusions.

## 2 Distinguished trajectories: a definition

First we start recalling the definition of distinguished hyperbolic trajectory provided in [17] for a system as follows:

$$\frac{d\mathbf{x}}{dt} = \mathbf{D}\mathbf{x} + g^{NL}(\mathbf{x}, t) \quad \mathbf{x} \in \mathbb{R}^n \quad (1)$$

Let  $\mathbf{x}(t)$  be a trajectory of Eq. (1) that remains in a bounded region for all time. Then  $\mathbf{x}(t)$  is said to be a distinguished hyperbolic trajectory if:

1. it is hyperbolic,
2. there exists a neighborhood  $\mathcal{B}$  in the flow domain having the property that the DHT remains in  $\mathcal{B}$  for all time, and all other trajectories starting in  $\mathcal{B}$  leave  $\mathcal{B}$  in finite time, as time evolves in either a positive or negative sense,
3. it is not a hyperbolic trajectory contained in the chaotic invariant set created by the intersection of the stable and unstable manifolds of another hyperbolic trajectory.

**Remark 1** *If the data spans only a finite time interval, then the DHT cannot be determined uniquely. Instead, there is a small region in  $\mathcal{B}$  where the DHT can exist.*

In [17] this setup is extended for general vector fields by means of coordinate transformations trying to recover the structure given in Eq. (1) and then applying the previous definition.

We construct now our definition of distinguished trajectory for a general vector field:

$$\frac{d\mathbf{x}}{dt} = \mathbf{v}(\mathbf{x}, t), \quad \mathbf{x} \in \mathbb{R}^n, t \in \mathbb{R} \quad (2)$$

in which we assume that  $\mathbf{v}(\mathbf{x}, t)$  is  $C^r$  ( $r \geq 1$ ) in  $\mathbf{x}$  and continuous in  $t$ . This will allow for unique solutions to exist, and also permit linearization, although linearization will not be used in our construction.

Before giving our definition of DT, we need first to introduce some notions and definitions. Let  $\mathbf{x}(t)$  denote a trajectory of the system (2) and let denote its components in  $\mathbb{R}^n$  as  $(x_1, x_2, \dots, x_n)$ . For all initial conditions  $\mathbf{x}^*$  in an open set  $\mathcal{B} \in \mathbb{R}^n$  consider the function  $M(\mathbf{x}^*)_{t^*, \tau} : \mathcal{B} \rightarrow \mathbb{R}$

$$M(\mathbf{x}^*)_{t^*, \tau} = \left( \int_{t^* - \tau}^{t^* + \tau} \sqrt{\sum_{i=1}^n \left( \frac{dx_i(t)}{dt} \right)^2} dt \right), \quad (3)$$

$M$  is the function that associates to each condition  $\mathbf{x}^*$  in  $\mathcal{B}$ , the arclength of the trajectory that passes through  $\mathbf{x}^*$  at time  $t^*$ . The arclength of the trajectory is considered over its projection in the phase space  $(x_1, x_2, \dots, x_n)$  and depends on  $t^*$  and  $\tau$ . The function  $M$  which is defined over an open set does not contain necessarily a minimum but if it exists is denoted by  $\min(M(\mathbf{x}^*)_{t^*, \tau})$ .

**Definition 2** ( $\tau$ -Distinguished trajectory). *A trajectory  $\gamma(t)$  of Eq. (2) is  $\tau$ -distinguished at time  $t^*$  if there exists an open set  $\mathcal{B}$  around  $\gamma(t^*)$  where the defined function  $M(\mathbf{x}^*)_{t^*, \tau}$  has a minimum and*

$$\min(M(\mathbf{x}^*)_{t^*, \tau}) = M(\gamma(t^*))_{t^*, \tau} \quad (4)$$

## 2.1 A discussion of the definition

The elements of the above definition deserve a detailed justification. We illustrate our explanations with examples in 1D. First we consider an example taken from [17, 22]. It is a linear one dimensional non autonomous dynamical system given by:

$$\frac{dx}{dt} = -x + t \quad (5)$$

For this example we consider the DHT reported as such in [17], which is given by  $x = t - 1$ . This is the particular solution of the linear equation (5) towards which all trajectories decay. The solution through the point  $x^*$  at  $t = 0$  is given by,

$$x(t) = t - 1 + e^{-t}(x^* + 1). \quad (6)$$

Figure 1a) displays several trajectories starting at time  $t = 0$  until  $t = 4$  and figure 1b) displays the same but from time  $t = -4$ . For each condition the function  $M$  provides the length of the projection of the trajectory over the  $x$ -axis in the range of times  $[-\tau, \tau]$ . Geometrically it is clear that in this example the function  $M$  should have a minimum at certain  $x$  value and that this value depends on  $\tau$ . We would like that the minimum of  $M$  coincides with the position of the DHT (the particular solution) at  $t = 0$ , however this would not be possible if in the definition of  $M$  only positive times are considered, *i.e.* if the limits of the integration were  $(0, \tau)$  the dashed trajectory in figure 1b) would have a lower projection in positive times than the particular solution. Analogously would have happened if only negative times would have been considered, that is if the limits of the integration would have been  $(-\tau, 0)$ . To determine precisely the position of the DHT at  $t = 0$ , both positive and negative times must be considered in the definition of  $M$ . Figure 2a) displays the function  $M(x^*)_{t=0,\tau}$  evaluated along trajectories of Eq. (6), at several  $\tau$  values. Figure 2b) displays the position of the minimum of the function  $M_{t=0,\tau}$  as a function of  $\tau$ . These minima correspond to the positions of the  $\tau$ -distinguished trajectories at  $t = 0$  and as  $\tau$  increases they approximate the coordinate of the DHT at this time, which is at  $x^* = -1$ . The pair  $(t^l, \mathbf{x}^l)$  formed by the time at which  $M$  is computed and the value of the coordinate  $\mathbf{x}^l$  to which the minimum of the function  $M_{t^l,\tau}$  for increasing  $\tau$  converges is called *limit coordinates*. The graphic 2b) illustrates the idea of approaching a point  $(t_0, \mathbf{x}_0)$  of the distinguished trajectory



by means of the *limit coordinates*.

Figure 2b) rises the question: what controls the convergence rate of the minima of  $M$  to the coordinates of the DHT? It is hard to answer rigorously this question for a general vector field as that of Eq. (2). Some insights may be provided however by particular examples. For instance the system:

$$\frac{dx}{dt} = -2x + 2t - 1, \quad (7)$$

presents the same DT than (5). Its solution through the point  $x^*$  at  $t = 0$  is given by,

$$x(t) = t - 1 + e^{-2t}(x^* + 1). \quad (8)$$

Now the decay of the solution towards the DHT is faster due to the presence of the exponential term  $e^{-2t}$  and figure 3 shows that in this case also the convergence rate of the minima of  $M$  towards the coordinates of the DHT at time  $t = 0$  is faster than before. However there exist systems in which the exponential decay of the solution is not a determining factor affecting the convergence rate of the minima of  $M$  towards the coordinates of the DHT. For instance in autonomous systems fixed points are the DTs, and clearly they are minimizers of  $M$  for any  $\tau > 0$  no matter what the exponential decay or growth rate of the nearby solution is.

In these examples the function  $M$  has a unique minimum, but as we will see this could not be so simple when nonlinearities are involved in the vector field. Also it is important to notice that the function  $M$  obtained at different  $\tau$  values has been used to obtain the *limit coordinates*  $(t_0^l, \mathbf{x}_0^l)$  and that these approach the  $\mathbf{x}_0$  coordinate of DHT *at a given time*  $t_0$  (here  $t_0 = t_0^l$ ). Once this is obtained, approaching the DHT at later times  $t_k = t_0 + k\Delta t$  would require to apply the same procedure to get the *limit coordinates*  $(t_k^l, \mathbf{x}_k^l)$ . We remark here that the proposed algorithm does not ensure that the set of *limit coordinates*

$(t_k^l, \mathbf{x}_k^l)$  are in fact part of a trajectory. Later we will see that in practice those points are approaching a true trajectory in many examples, however in realistic aperiodic flows this has to be verified *a posteriori*. These considerations lead us to the definition of *Distinguished Trajectory*

**Definition 3** (*Distinguished trajectory*). *A trajectory  $\gamma(t)$  is said to be Distinguished within accuracy  $\epsilon$  ( $0 \leq \epsilon$ ) in a time interval  $[t_0, t_N]$  if there exists a continuous path of limit coordinates  $(t^l, \mathbf{x}^l)$  where  $t^l \in [t_0, t_N]$ , such that,*

$$\|\gamma(t^l) - \mathbf{x}^l(t^l)\| \leq \epsilon, \quad \forall t^l \in [t_0, t_N] \quad (9)$$

where  $\|\cdot\|$  represents the distance defined as,

$$\|\mathbf{a} - \mathbf{b}\| = \sqrt{\sum_{i=1}^n (a_i - b_i)^2} \quad \text{with } \mathbf{a}, \mathbf{b} \in \mathbb{R}^n$$

In the numerical exploration of this definition we will replace the continuous path of *limit coordinates*  $(t^l, \mathbf{x}^l)$  and the continuous trajectory  $\gamma(t)$  by a discrete representation  $(t_k^l, \mathbf{x}_k^l)$  and  $\gamma(t_k^l)$  where  $t_0 \leq t_k^l \leq t_N$ . In practice, from definition 3 follows that any trajectory could be distinguished if  $\epsilon$  is large enough, however the interesting distinguished trajectories are those for which  $\epsilon$  is close to zero, which means it is of the order of the accuracy in which  $\gamma(t_k^l)$  and  $\mathbf{x}^l(t_k^l)$  are numerically determined, or zero, if an exact expression for both is known.

Finally we discuss some remarks. First, it is not guaranteed that a path of *limit coordinates* is a trajectory, although if that is the case then from definition 3 follows that this trajectory is distinguished. Second, one could think that if *limit coordinates* at  $t_0$  are found that approach within a great accuracy a point of *an existing DT*, the iterative procedure described above to find a set of *limit coordinates*  $(t_k^l, \mathbf{x}_k^l)$  approaching the DT at later times is an unnecessary computational effort, as those coordinates could have been equally obtained just by integrating forwards the initial data. However there exist examples as

for instance a hyperbolic DT in 2D with an unstable manifold, that cannot be integrated like this, as the integrated trajectory will eventually leave the neighborhood of the DT through the unstable manifold no matter what small the error in the initial data is. We will address these issues in detail in next sections.

### 3 A numerical algorithm

In this section we propose an algorithm to compute a path of *limit coordinates* in a time interval, and we verify that it is close to a DT of a known example. For this purpose we compute, at successive increasing  $\tau$  values, the minimum of the function  $M_{t=0,\tau}(\mathbf{x})$  for  $\mathbf{x}$  in an open set in  $\mathbb{R}^n$ . The method is illustrated in a 2D case, the periodically forced Duffing:

$$\begin{aligned}\dot{x} &= y, \\ \dot{y} &= x - x^3 + \varepsilon \sin(t),\end{aligned}\tag{10}$$

where  $\varepsilon$  is a parameter. The hyperbolic fixed point of the unperturbed autonomous system (i.e.,  $\varepsilon = 0$ ) is at the origin  $\mathbf{x} = (0, 0)$ . For small  $\varepsilon$ , it is possible to compute by perturbation theory (see [23]), the following periodic trajectory which stays close to the origin:

$$\mathbf{x}_{DHT}(t) = -\frac{\varepsilon}{2} \begin{pmatrix} \sin t \\ \cos t \end{pmatrix} - \frac{\varepsilon^3}{40} \begin{pmatrix} 2 \sin^3 t + \frac{3}{2} \sin t \cos^2 t \\ \frac{3}{2} \cos^3 t + 3 \sin^2 t \cos t \end{pmatrix} + \mathcal{O}(\varepsilon^5).\tag{11}$$

For  $\varepsilon = 0.1$  Eq. (11) provides an accuracy up to the fifth digit. This trajectory is identified as *Distinguished* in Ref. [17], for this reason we have labeled it as *DHT*. Replacing the expression,

$$\mathbf{x} = (x, y) = \mathbf{x}_{DHT}(t) + (\xi_1, \xi_2)\tag{12}$$

into Eq. (10) and dropping the nonlinear terms one finds that the linearized equations have two linearly independent solutions in terms of which the time

evolution of the components  $(\xi_1, \xi_2)$  is:

$$(\xi_1, \xi_2) = \alpha e^t \begin{pmatrix} 1/\sqrt{2} \\ 1/\sqrt{2} \end{pmatrix} + \beta e^{-t} \begin{pmatrix} -1/\sqrt{2} \\ 1/\sqrt{2} \end{pmatrix} + \mathcal{O}(\varepsilon^2). \quad (13)$$

Eq. (13) confirms the hyperbolicity of the solution (11).

The explicit expression of the distinguished hyperbolic trajectory is a benchmark to test the utility of our definition. The procedure starts by determining the coordinates of  $\mathbf{x}_{DHT}$  at time  $t = 0$ . We consider an open set  $\mathcal{D} \subset \mathbb{R}^2$ ,  $\mathcal{D} = (-0.2, 0.2) \times (-0.2, 0.2)$  and  $\tau$  is 2 in the function  $M_{t=0, \tau}(\mathbf{x})$ . Figure 4 displays a contour plot of  $M_{t=0, \tau=2}(\mathbf{x})$  which has the minimum at  $\mathbf{x} = (0, -5.7057 \cdot 10^{-2})$ . As noted in previous section, by increasing the  $\tau$  value, the position of the minimum becomes closer and closer of the coordinates of the DHT at  $t = 0$ . Figure 5 shows contour plots of the function  $M$  at several  $\tau$  values. Fig. 5a) displays a typical hyperbolic structure of  $M$  for  $\tau = 5$  where the directions of the stable and unstable manifolds are recognized. The function  $M$  presents a unique minimum in Fig. 5a) at  $\mathbf{x} = (0, -4.979 \cdot 10^{-2})$  while several appear for  $\tau = 10$  in Fig. 5b). The global minimum in this picture corresponds to  $\mathbf{x} = (0, -5.0042565261 \cdot 10^{-2})$ . Figure 6a) compares the  $x$ -coordinate of  $\mathbf{x}_{DHT}$  as a function of time with trajectories with initial conditions at the global minimum of  $M_{t=0, \tau=2}$  and  $M_{t=0, \tau=10}$ . Considering as initial condition the global minimum of  $M_{t=0, \tau}$  for  $\tau = 10$  provide a trajectory that stays close to  $\mathbf{x}_{DHT}$  for a larger time interval than for  $\tau = 2$ , thus confirming that larger  $\tau$ -values approach better and better the coordinates of the DHT. Fig. 5c) displays the contour plot of  $M_{t=0, \tau=50}(\mathbf{x})$ , its global minimum is at  $\mathbf{x} = (0, -5.0037606418 \cdot 10^{-2})$ . The associated trajectory depicted in Fig. 6b) shows that this initial condition tracks the DHT in a larger time interval than those obtained for  $\tau = 2$  and 10, however the figure shows that the integration of the DHT in  $(-50, 50)$  is not possible, in fact the associated trajectory stay close to the DHT just in the time interval  $(-20, 20)$ . This confirms that results

obtained for  $\tau = 50$  are the same to those obtained for  $\tau = 20$ . In practice for a finite precision numerical scheme, as the one used here which is a 5th order Runge Kutta, the approach to the DHT has an upper bound on  $\tau$ , since the stable and unstable manifolds of the hyperbolic trajectory magnify any initial error either in negative or positive time and beyond this  $\tau$ -limit numerical errors dominate. The convergence towards the DHT is confirmed in Fig. 7 which displays the evolution of the coordinates  $x$  and  $y$  of the global minimum of  $M$  as a function of the parameter  $\tau$ .

The new minima appearing in Figs. 5b) and c) address the existence of different  $\tau$ -distinguished trajectories. They correspond to trajectories which stay close to  $\mathbf{x}_{DHT}$  in a small time range within the interval  $-\tau < t < \tau$ , but afterwards as illustrated in Fig. 6b), they fly apart from the DHT.

We describe now a numerical scheme to compute a path of limit coordinates. The algorithm has the following steps:

1. Step 1. Discretize the domain  $\mathcal{D}$  at the initial time  $t = t_0$  at which one wishes to compute a DT. For instance the grid size of this domain in Fig. 4 is  $101 \times 101$ . The function  $M$  is evaluated at each grid point for a given  $\tau_0$ .
2. Step 2. Search for the local minima of  $M_{t_0, \tau_0}$  in the interior of the grid. These minima approach the coordinates of  $\tau_0$ -distinguished trajectories within the accuracy of the grid. In what follows we restrict our description to a unique minimum as it simplifies the description and the procedure is easily generalized to a multiple case.
3. Step 3. Improve the approach of the coordinates of the  $\tau_0$ -distinguished trajectory up to precision  $\delta$ . For this purpose centred in the candidate point provided by step 2, build up a  $3^n$  grid (for the 2D case this is a  $3 \times 3$  grid as Fig. 8 illustrates) setting the distance between nodes equal

to  $\delta$ . Then evaluate  $M_{t_0, \tau_0}$  at the points of the  $\delta$ -grid. If the minimum of  $M_{t_0, \tau_0}$  is in the interior of the grid, then the coordinates of the  $\tau_0$ -distinguished trajectory are known within  $\delta$  accuracy, otherwise the  $\delta$ -grid must be rebuilt centred on the boundary point where the minimum has been located, and  $M_{t_0, \tau_0}$  must be re-evaluated in the new  $\delta$ -grid. This procedure stops when the minimum of  $M_{t_0, \tau_0}$  is in the interior of the grid.

4. Step 4. Computing the *limit coordinates* at time  $t_0$ . Define a sequence of increasing  $\tau$ -values as follows:  $\tau_1 = \tau_0 + \Delta\tau$  and  $\tau_2 = \tau_0 + 2\Delta\tau$ . Then evaluate  $M_{t_0, \tau_0}$ ,  $M_{t_0, \tau_1}$  and  $M_{t_0, \tau_2}$  at the  $\delta$ -grid. If the minimum is at the interior position for the three cases, then we consider that *limit coordinates* have been found within  $\delta$  accuracy. We note that this is a necessary but not sufficient condition as one does not know a priori how is the convergence rate to the distinguished trajectory. However, although this criterion could be strengthened, it has been tested and found to be appropriated in the examples explained in next sections. If the condition defined above of getting a minimum at an interior position for the sequence of  $\tau$ -values is not satisfied then, after replacing  $\tau_0$  by  $\tau_1$ , we return to step 3 and then to step 4. The loop between steps 3 and 4 is stopped when the condition of step 4 is satisfied for some  $\tau_k$ .
5. Step 5. Compute the *limit coordinates* at time  $t_1 = t_0 + \Delta t$ . Once the *limit coordinates* have been approached at time  $t_0$ , they are forward integrated with the numerical method in use up to time  $t_1$ . If the *limit coordinates* converge to an hyperbolic DT with an unstable manifold, the position  $\mathbf{x}(t_1)$  obtained should be deviated from the position of the DT at time  $t_1$ . In order to correct this, the procedure described above is repeated from step 3 onwards. For that purpose in the definition of  $M$ ,  $t_0$  is replaced by  $t_1$  and the  $\tau$ -value is reset to  $\tau_0$ . The coordinates  $\mathbf{x}(t_1)$  are the first

approximation to the  $\tau_0$ -distinguished trajectory at time  $t_1$ . Once the *limit coordinates* are conveniently approached at time  $t_1$  it is possible to repeat the procedure to locate them at successive times  $t_2, t_3, \dots, t_N$ .

The explained algorithm requires as an input: an explicit expression of the dynamical system (2); the definition of the domain  $\mathcal{D} \subset \mathbb{R}^n$ ; the initial and final times  $t_0, t_N$  at which DHTs are required and the time step  $\Delta t$  for intermediate times; the initial  $\tau_0$  and the increment  $\Delta\tau$ ; the  $\delta$  precision. As an output the algorithm provides: a path of limit coordinates at the selected times  $t_k$ .

Next we discuss in more detail some technical aspects related to the implementation of the above algorithm. Steps 1 and 3 require evaluating  $M_{t_0, \tau_0}$  as defined in Eq. (3). We explain how this is done for the contours plots displayed in Figs. 4 and 5 which are referred to the system (10) at  $t_0 = 0$ . Fig. 9 shows a schematic projection onto the  $\mathbb{R}^2$  plane of a possible trajectory  $\mathbf{x}(t)$  of the system from  $-\tau$  to  $\tau$ . As it is numerically obtained only a finite number of points ( $L$ ) appear. This picture suggest the following discrete version of Eq. (3) for  $M$ :

$$M(\mathbf{x})_{0, \tau} = \sum_{j=1}^{L-1} \left( \int_{p_i}^{p_f} \sqrt{\left(\frac{dx_j(p)}{dp}\right)^2 + \left(\frac{dy_j(p)}{dp}\right)^2} dp \right), \quad (14)$$

where the functions  $x_j(p)$  and  $y_j(p)$  represent a curve interpolation parametrized by  $p$ , and the integral:

$$\int_{p_i}^{p_f} \sqrt{\left(\frac{dx_j(p)}{dp}\right)^2 + \left(\frac{dy_j(p)}{dp}\right)^2} dp \quad (15)$$

is numerically computed. In our case we use the Romberges method (see [25]) of  $2K$  order with  $K = 5$ . It is clear that accuracy on the evaluation of  $M$  will depend on the number of points on the trajectory  $L$ , which is controlled by the time step size of the integrator (a 5th order Runge Kutta method) and on the interpolation scheme between points. Two interpolation methods are compared in tables (1) and (2). Results in table (1) are obtained with a linear inter-

polation between nodes. Results in table (2) corresponds to the interpolation method used by Dritschel [26] in the context of contour dynamics and that has been successfully applied in [23] to the computation of invariant manifolds in aperiodic flows. This method interpolates a piece of the curve in Fig. 9 between consecutive nodes as follows:

$$\mathbf{x}_j(p) = \mathbf{x}_j + p\mathbf{t}_j + \eta_j(p)\mathbf{n}_j \quad (16)$$

for  $p_i = 0 \leq p \leq p_f = 1$  with  $\mathbf{x}_j(0) = \mathbf{x}_j$  and  $\mathbf{x}_j(1) = \mathbf{x}_{j+1}$ , where:

$$\mathbf{t}_j = (a_j, b_j) = \mathbf{x}_{j+1} - \mathbf{x}_j, \quad \mathbf{t}_j \in \mathbb{R}^2 \quad (17)$$

$$\mathbf{n}_j = (-b_j, a_j), \quad \mathbf{n}_j \in \mathbb{R}^2 \quad (18)$$

$$\eta_j(p) = \mu_j p + \beta_j p^2 + \gamma_j p^3, \quad \eta_j \in \mathbb{R}. \quad (19)$$

The cubic interpolation coefficients  $\mu_j$ ,  $\beta_j$  and  $\gamma_j$  are

$$\mu_j = -\frac{1}{3}d_j\kappa_j - \frac{1}{6}d_j\kappa_{j+1}, \quad \beta_j = 2d_j\kappa_j, \quad \gamma_j = \frac{1}{6}d_j(\kappa_{j+1} - \kappa_j),$$

where  $d_j = |\mathbf{x}_{j+1} - \mathbf{x}_j|$  and

$$\kappa_j = 2 \frac{a_{j-1}b_j - b_{j-1}a_j}{|d_{j-1}^2\mathbf{t}_j + d_j^2\mathbf{t}_j - 1|}$$

is the local curvature defined by a circle through the three points,  $x_{j-1}$ ,  $x_j$ , and  $x_{j+1}$ .

Tables (1) and (2) show errors on the computed lengths of ellipses at different ratios between the major and minor axis. The reference length is that obtained with GNU Octave version 2.1.73, as it provides 16 correct digits for the known case of the circumference. Tables confirm that Dritschel method is superior to linear interpolation and for this reason that is the one used to compute the function  $M$ . In the trajectory from  $-\tau$  to  $\tau$  the number of points  $L$  is determined by the time step size of the Runge Kutta method which is set to  $10^{-2}$ .

Another important element of the algorithm for discussion is the value of the input parameters, specially of  $\tau_0$  and  $\Delta\tau$ . It is clear from Fig. 5 that



large  $\tau$  values are not convenient as they increase the roughness of the function  $M$  and several local minima may appear in the neighbourhood of a DHT that correspond to trajectories that stay for some time close to it. On the other hand it is clear that large enough  $\tau$  values are required to fix the coordinates of the DHT within certain accuracy. Conjugating these aspects suggest the use of relatively small values for the initial  $\tau_0$ . In the example above  $\tau_0 = 2$ , allows to get as a starting point a smooth  $M$  as that of Fig. 4. The increments should not be too large, in practice we have chosen  $\Delta\tau = \tau_0/2$ , this prevents from stepping to a too rough  $M$  before getting close enough to the searched DHT. Some of the local minima appearing in Fig. 5b) are just apparent and disappear in a more accurate grid, however others as already noticed, belong to true  $\tau$ -distinguished trajectories, which are secondary and can be avoided if the increment of the  $\tau$ -values is conveniently small. These choices are found to be appropriate to determine with great accuracy the DHT in (11) by means of a path of *limit coordinates*. Figure 10a) represents both the analytical DHT and the numerical limit coordinates and Figure 10b) displays the distance between the exact and the numerical approach, confirming that the DHT in (11) is also a DT following our definition 3 within accuracy  $\epsilon = 10^{-6}$ . Other parameters in the algorithm are  $\delta = 10^{-6}$ , step size in the Runge Kutta method  $10^{-2}$ ,  $\Delta t = 0.01$ ,  $t_0 = 0$  and  $t_N = 6$ . To locate the DHT within accuracy  $\delta = 10^{-6}$  requires increasing  $\tau$  up to values of 15, which is near the limit of the integration method. Figure 11 shows the maximum  $\tau$  required at each  $t_k$ .

## 4 Applications to exact examples

In this section we apply the algorithm explained in the previous section to selected examples in 2D.

## 4.1 A non hyperbolic distinguished trajectory

The unperturbed autonomous system (10) obtained with  $\varepsilon = 0$  has two non hyperbolic fixed points at  $(-1, 0)$  and  $(1, 0)$ . Obviously these fixed points correspond to DT which are also  $\tau$ -distinguished trajectories for all  $\tau > 0$ . For the periodically forced system (10) with small  $\varepsilon$  it is possible to find close to those fixed points by perturbation theory periodic solutions in a similar way to the hyperbolic one discussed in previous section. For instance close to the point  $(1, 0)$  we find this periodic trajectory:

$$x_{DET}(t) = -\begin{pmatrix} 1 \\ 0 \end{pmatrix} + \varepsilon \begin{pmatrix} \sin t \\ \cos t \end{pmatrix} + 3\varepsilon^2 \begin{pmatrix} \frac{1}{2} \cos^2 t \\ -\sin t \cos t \end{pmatrix} + \mathcal{O}(\varepsilon^3). \quad (20)$$

This solution has not been addressed as *Distinguished* in previous works [17, 18], as these have been focused in hyperbolic trajectories and this one, as proved next, is not hyperbolic. However we have labeled it as *DET* anticipating its *Distinguished* property for two reasons. One is that it is periodic, and we expect periodic orbits to be distinguished, and second is that it is in clear correspondence to the elliptic fixed point  $(-1, 0)$  in the limit  $\varepsilon = 0$ , and fixed points are DT.

To determine the stability of (20) we proceed as before, by replacing the expression

$$\mathbf{x} = (x, y) = \mathbf{x}_{DET}(t) + (\xi_1, \xi_2) \quad (21)$$

into Eq. (10). We find that the system linearized system at order  $\varepsilon^0$  is:

$$\frac{d\xi_1}{dt} = \xi_2 \quad (22)$$

$$\frac{d\xi_2}{dt} = -2\xi_1 \quad (23)$$

Therefore the linearized flow around  $\mathbf{x}_{DET}(t)$  evolves according to:

$$(\xi_1, \xi_2) = \alpha e^{i\sqrt{2}t} \begin{pmatrix} 1/\sqrt{3} \\ i\sqrt{2/3} \end{pmatrix} + \alpha^* e^{-i\sqrt{2}t} \begin{pmatrix} 1/\sqrt{3} \\ -i\sqrt{2/3} \end{pmatrix} + \mathcal{O}(\varepsilon) \quad (24)$$

which clearly is non hyperbolic.

We apply our algorithm to determine the *limit coordinates* approaching (20), as we want to verify whether the definition 3 is also at work for time dependent non hyperbolic solutions. The following input is considered:  $\mathcal{D} = (-1.2, -0.8) \times (-0.2, 0.2)$ ,  $\tau_0 = 2$ ,  $\Delta\tau = 1$ ,  $\delta = 10^{-4}$ ,  $t_0 = 0$ ,  $t_N = 6$  and time step of the Runge-Kutta integrator  $10^{-2}$ . We note that the accuracy  $\delta$  is not as demanding as before, since now  $\mathbf{x}_{DET}$  for  $\varepsilon = 0.1$  is only accurate up to the third digit. Figure 12 shows a rather different structure for the function  $M$ . An important feature is the smoothness of  $M$  close to the DET even for large  $\tau$ . In figure 12b) are remarkable the differences between the rather flat region around the position of the DT given by (20), which appears in the dark tone, and the roughness of the outer part. The irregularity of this region suggest that inside it nearby trajectories follow rather different paths as it happens in chaotic motions, while the regularity of the central core suggest the existence of trapped trajectories circling around the DET. On this perspective the function  $M$  at large  $\tau$  seems a useful tool to fix the boundaries of a Lagrangian eddie, different to those proposed in [27, 29].

Fig. 13 shows the convergence rate of the global minimum of  $M$  in the domain  $\mathcal{D}$  as a function of  $\tau$ . The convergence towards the coordinates of the DT is oscillatory and rather slow since  $\tau$  values up to 600 are required. A slight difference between the exact coordinates of the DT and the numerically computed limit coordinates is appreciated, however we recall here that these differences are consistent with the precision in which the exact DT is known, which is only up to the third digit. Figure 14, and more specifically figure 14b), confirms that the exact expression in Eq. (20) is in fact a distinguished trajectory according to our definition 3 within accuracy  $\epsilon = 4 \cdot 10^{-3}$ .

Figure 15a) shows a forward and backward integration along the time interval  $(-50, 50)$  taking as initial data the limit coordinates supplied by our algorithm

at time  $t_0 = 0$ , and compares it with the exact solution of the DT. From figure 15b) is observed that this trajectory evolves close to the exact solution in whole time range. This result shows that contrary to what happens near hyperbolic trajectories, in the nearby of non hyperbolic trajectories, any small error does not amplify and as consequence once a DT *is known to exist* it could have been computed just by integrating forwards and backwards the limit coordinates found at a given time  $t_k$ . However one needs to be careful here, as a trajectory is not necessarily distinguished at all times, and for it be named properly as distinguished one should verify that it stays close to the *limit coordinates* in the whole time interval, and therefore one cannot avoid computing *limit coordinates* along the time interval in this case either. We will come again to this point in next section.

## 4.2 The rotating Duffing equation

We analyze next the aperiodic hyperbolic distinguished trajectory of a system already studied in [23], the rotating Duffing equation:

$$\begin{pmatrix} \dot{\eta}_1 \\ \dot{\eta}_2 \end{pmatrix} = \begin{pmatrix} \sin 2\omega t & \cos 2\omega t + \omega \\ \cos 2\omega t - \omega & -\sin 2\omega t \end{pmatrix} \begin{pmatrix} \eta_1 \\ \eta_2 \end{pmatrix} + (\varepsilon \sin t - [\cos \omega t \eta_1 - \sin \omega t \eta_2]^3) \begin{pmatrix} \sin \omega t \\ \cos \omega t \end{pmatrix}. \quad (25)$$

This Duffing equation is quasi-periodic in time when the rotation rate  $\omega$  is irrational. It is obtained from the system (10) by applying the linear, rotation coordinate transform  $\mathbf{x} = R(t)\boldsymbol{\eta}$ , where

$$R(t) = \begin{pmatrix} \cos \omega t & -\sin \omega t \\ \sin \omega t & \cos \omega t \end{pmatrix}. \quad (26)$$

The DHT can also be obtained through the coordinate transform:

$$\boldsymbol{\eta}_{DHT}(t) = R(t)^{-1}\mathbf{x}_{DHT}(t), \quad (27)$$

Figure 16, and in particular Fig. 16b) confirms that the DHT of Eq. (27) is also a DHT according to our definition 3 within accuracy  $\epsilon = 4 \cdot 10^{-6}$ .

## 5 Application to vector fields defined as finite time data sets

In this section we explore definition 3 in a highly aperiodic flow in which the vector field is defined as a finite time data set. In particular we consider the output of a quasigeostrophic wind-driven double gyre model in a regime already studied in [11, 12]. Details of this model may be found in [12, 21]. Fig. 17 shows a typical output of the streamfunction provided by this model. The velocity data set is obtained on a 1000 km  $\times$  2000 km rectangular domain and spans over 4000 days. This interval is considered after the fluid is started from rest and allowed to spin up for 25000 days. Free slip conditions are considered for the velocity on the boundaries and the wind stress curl is 0.32 dyn/cm<sup>2</sup>. The equations of motion for this system are given by:

$$\dot{x} = v_x(x, y, t) = -\frac{\partial\psi}{\partial y}, \quad (28)$$

$$\dot{y} = v_y(x, y, t) = \frac{\partial\psi}{\partial x}, \quad (29)$$

and the variables  $x$  and  $y$  are in the rescaled domain  $[0, 1] \times [0, 2]$ . Here the velocity fields  $v_x$  and  $v_y$  are provided as a finite time data set and are interpolated using bicubic interpolation in space and 3rd order Lagrange polynomials in time. This method has been reported to be good enough to integrate trajectories in [24]. We will focus our analysis in the time interval  $[0, 900]$  in the area marked by a rectangle in Fig. 17 for which [12] reports the computations of several DHT. In [12] distinguished trajectories are computed by means of an iterative algorithm which is initialized on a hyperbolic instantaneous stagnation point (ISP). In particular two paths of such ISP are chosen in the Northern gyre in the time intervals  $[0, 339]$  and  $[446, 880]$ . From each of these paths, a DHT is computed which are in the same geographical area although their coordinates are determined in a different time range. In Fig. 18 we show the  $x$

and  $y$  evolution for these trajectories. These coordinates have been computed with a different algorithm to that proposed in [12], instead each correspond to a trajectory which is in the intersection of a piece of stable manifold and a piece of unstable manifold which are time evolved backwards and forwards respectively. In this procedure, in order to avoid the numerous intersections between stable and unstable manifolds, which difficult the tracking of the trajectory which is distinguished, manifolds are trimmed at each time step following the method described in [11] where one branched manifolds are computed. This method is taking advantage of the fact that a DHT must be in the intersection of both manifolds at all times, as it is a trajectory, however does not improve the method explained in [12] in the sense that does not allow either to extend the computation of the DHT beyond the time interval in which the ISP exists. Many questions have been raised for these trajectories as discussed in [11, 12]. For instance as they have been computed only on a finite time interval where the ISP exist, one can ask how to pursue its computation beyond that interval. Another open discussion in [12] concerns to deciding if the two DHT in Fig. 18 computed at different times are part of the same or are a different trajectory. In [11] is raised the question about the possibility of a DHT ceasing being distinguished or hyperbolic. In this section we apply our algorithm to compute limit coordinates and verify whether trajectories in Fig. 18 are distinguished or not following our definition 3. Also we will describe the insights of this definition into those questions raised in [11, 12]. We have applied our algorithm to compute limit coordinates in the domain in which the DHT shown in Fig. 18a) exists. In particular we have applied it with the input:  $\mathcal{D} = (55, 75) \times (1325, 1375) \text{ km}^2$ ,  $t_0 = 120$ ,  $t_N = 300$ ,  $\Delta t = 5$  days,  $\tau_0 = 2$  days,  $\Delta\tau = 5$  days and  $\delta = 10^{-3}$  km. The time step of Runge-Kutta method is 0.1 days. Fig. 19a) shows with a solid line the projection onto the  $x - y$  plane of the trajectory depicted in figure 18a) in the interval (120, 300), and with circles the path of limit coordi-

nates. Fig. 19b) shows the evolution of the distances between these trajectories. This confirms that the trajectory displayed in Fig. 18a) is also distinguished regarding definition 3 in the time interval  $[120, 330]$  within accuracy  $\epsilon = 8 \cdot 10^{-1}$  km. Thus in this time interval, limit coordinates are a method to compute DT different to those proposed in [12, 17]. Circles in Fig. 20 show the location of the  $x$  limit coordinates computed with our algorithm versus time. The solid line represents a trajectory obtained after integrating with a 5th order Runge-Kutta method forwards and backwards in time the initial condition of the circle at day 285. The dashed line represents the same, but with the initial condition slightly perturbed. It is appreciated that in both cases trajectories are aligned with the path of limit coordinates. The distinguished trajectory is highly hyperbolic backwards in time as a small perturbation greatly amplifies in that sense, while it does not do forwards in time, suggesting that it has a non hyperbolic type of stability in that sense (see comments to Figs. 6 and 15).

Beyond day 300 it is possible to continue the path of limit coordinates. Figure 21 shows a diagram at day 330 where it is shown the convergence of the  $x$  component of the minimum of  $M$  versus  $\tau$ . This type of convergent diagrams are not found in this neighborhood for day 337. On the other hand, although it is possible to continue the path of limit coordinates beyond day 300, Fig. 22 proves that this path is not a trajectory. There it is appreciated the existence of different trajectories crossing the path, confirming that it is not a trajectory as otherwise it would violate the unicity of the solution. Therefore, following our construction it is possible to say that beyond day 300 the trajectory is not longer distinguished with a small accuracy.

Fig. 23 confirms that trajectory in Fig. 18b) is also distinguished according to definition 3 in the time interval  $(470, 860)$  within accuracy  $\epsilon = 3$  km. In particular to compute the path in Fig. 23 we have applied the algorithm of section 3 with the input:  $\mathcal{D} = (50, 65) \times (1255, 1270)$  km<sup>2</sup>,  $t_0 = 470$ ,  $t_N = 860$ ,

$\Delta t = 5$  days,  $\tau_0 = 2$  days,  $\Delta\tau = 7$  days and  $\delta = 10^{-3}$  km. The time step of the Runge-Kutta method is 0.1 days. In the time interval from day 600 to day 650 due to the presence of nearby elliptic type minima in the function  $M$ , that were difficulting the track of the path of limit coordinates, some of the input parameters were modified as follows:  $\mathcal{D} = (73.5, 75.5) \times (1384, 1392)$  km<sup>2</sup>,  $\tau_0 = 40$  days and  $\Delta t = 1$  day.

Finally we discuss the existence of non hyperbolic distinguished trajectories in this data set. The presence of this type of trajectories has not been addressed before, and we do not have any benchmark solution. We have looked for this type of trajectory in areas of the flow where Eulerian eddies seemed to persist for long times. Figure 24 represents the function  $M$  at day 370 for  $\tau = 150$  and  $\tau = 250$ . In these figures it is appreciated the structure of an eddie at the centre even for rather long  $\tau$ -values, however figure 25 does not confirm the convergence of the minimum of  $M$  towards a constant value. On the other hand the slow convergence in diagram 13 towards the non hyperbolic trajectory, already had suggested that long time intervals were required for that purpose, and those intervals might be difficult to find in realistic flows as the one analyzed here.

## 6 Conclusions

In this paper we have proposed a new definition of distinguished trajectory that extends the concept of fixed point and periodic orbit to aperiodic dynamical systems. We have verified that this definition can be numerically implemented and that the procedure consist of determining a path of *limit coordinates*. We have analyzed exact examples in the Duffing equation with known distinguished trajectories both periodic and non periodic and we have found that the path of limit coordinates, within numerical accuracy, coincides with the distinguished



trajectories and therefore those trajectories are identified also as *distinguished* in the framework of our definition. As a novelty with respect to previous works dealing with distinguished trajectories, our definition is applicable to non-hyperbolic trajectories, in particular we have studied a periodic orbit of the Duffing equation with non hyperbolic stability and it has been also recognized as *distinguished* by our definition. In this case the function  $M$  from which the *limit coordinates* are computed, seems to be a suggestive tool to characterize Lagrangian eddies. We have tested our definition in the context of realistic aperiodic flows where distinguished hyperbolic trajectories had been found [12, 17]. Again we have identified these trajectories by paths of limit coordinates in certain time intervals. Beyond these time intervals the trajectories are not longer *distinguished* according to our definition. Thus in the context of the definitions provided in this paper the property of a trajectory of being *distinguished* may be lost in time. Also we have found evidence that the hyperbolicity of these trajectories is not constant in time. These two statements provide answers to the open questions mentioned in the text that had been addressed in [11, 12].

## Acknowledgements

Authors have been supported by CSIC grants PI-200650I224 and OCEANTECH (No. PIF06-059) and the Comunidad de Madrid project SIMUMAT S-0505-ESP-0158. It is a pleasure to acknowledge many useful conversations with Steve Wiggins, Des Small, Peter Haynes, Emilio Hernández-García, Cristóbal López, Antonio Turiel, Emilio García-Ladona, Michal Branicki and Wenbo Tang on numerous issues related to this subject. The computational part of this work has been done in CESGA computers SVGD and FINIS TERRAE and in the SIMUMAT-CSIC cluster ODISEA.

## References

- [1] Aref, H., 1984. Stirring by chaotic advection. *J. Fluid Mech.* 143, 1–21.
- [2] Khakhar DV, Ottino J.M. Fluid mixing (stretching) by time-periodic sequences for weak flows. *Physics of Fluids* 29 11 3503-3505 (1986).
- [3] Dombre T., Frisch U., Greene J.M., Henon M., Mehr A., Soward A.M. Chaotic Streamlines in the ABC flows *Journal of Fluid Mechanics* 167, 353-391 (1986).
- [4] Wiggins, S.: *Chaotic Transport in Dynamical Systems*, Springer-Verlag, New York, 1992
- [5] Wiggins, S.: *Introduction to Applied Nonlinear Dynamical Systems and Chaos*, Springer-Verlag, New York, 2003.
- [6] Guckenheimer, J., Holmes, P.: *Nonlinear Oscillations, Dynamical Systems, and Bifurcations of Vector Fields*, Springer-Verlag, New York, 2002
- [7] Malhotra, N. and Wiggins, S.: Geometric Structures, Lobe Dynamics, and Lagrangian Transport in Flows with Aperiodic Time Dependence, with Applications to Rossby Wave Flow, *J. Nonlinear Sci.*, 8, 401-456, 1998.
- [8] Haller, G. and Poje, A.: Finite time transport in aperiodic flows, *Physica D*, 119, 3/4, 352-380, 1998.
- [9] Langa JA, Robinson JC, Suarez A. Stability, instability, and bifurcation phenomena in non-autonomous differential equations. *Nonlinearity* 15 (3) 887-903 (2002).
- [10] Langa JA, Robinson JC, Suarez A. Bifurcations in non-autonomous scalar equations. *Journal of Differential Equations*. 221 (1) 1-35 (2006).

- [11] Mancho A. M., Small D., Wiggins S., A tutorial on dynamical systems concepts applied to Lagrangian transport in oceanic flows defined as finite time data sets: Theoretical and computational issues. *Physics Reports* 437, 3-4 (2006).
- [12] Mancho, A. M., Small, D., Wiggins, S., 2004. Computation of hyperbolic and their stable and unstable manifolds for oceanographic flows represented as data sets. *Nonlinear Process. Geophys.* 11, 17–33.
- [13] Mancho A. M., Hernández-García E., Small D., Wiggins S., Fernández V. Lagrangian transport through an ocean front in the North-Western Mediterranean Sea. *Journal of Physical Oceanography* 38, 6, 1222-1237 (2008).
- [14] Aurell E., Boffetta G., Crisanti A., Paladin G., Vulpiani A. Predictability in the large: an extension of the concept of Lyapunov exponent. *J. Phys. A: Math. General*, 30: 1-26, 1997.
- [15] Haller, G. Distinguished Material surfaces and coherent structures in three-dimensional fluid flows. *Physica D*, 149: 248-277, 2001.
- [16] Nese JM, Quantifying local predictability in phase space. *Physica D* 35: 237-250, 1989.
- [17] Ide, K., Small, D., Wiggins, S., 2002. Distinguished hyperbolic trajectories in time dependent fluid flows: analytical and computational approach for velocity fields defined as data sets. *Nonlinear Process. Geophys.* 9, 237–263.
- [18] Ju, N., Small, D., Wiggins, S., 2003. Existence and computation of hyperbolic trajectories of aperiodically time-dependent vector fields and their approximations. *Int. J. Bif. Chaos* 13, 1449–1457.
- [19] G. Haller. Exact theory of unsteady separation for two dimensional flows. *Journal of Fluid Mechanics* 512, 257-311 (2004)

- [20] Eisenbach S., Friedrich R., Large-eddy simulation of flow separation on an airfoil at a high angle of attack and  $Re=10^5$  using Cartesian grids. *Theoretical and Computational Fluid Dynamics* 22 (3-4) 213-225 (2008).
- [21] Coulliette, C., Wiggins, S., 2001. Intergyre transport in a wind-driven, quasigeostrophic double gyre: an application of lobe dynamics. *Nonlinear Process. Geophys.* 8, 69–94.
- [22] Szeri, A., Leal, L. G., and Wiggins, S.: On the Dynamics of Suspended Microstructure in Unsteady, Spatially Inhomogeneous Two-Dimensional Fluid Flows, *J. Fluid Mech.*, 228, 207241, 1991.
- [23] Mancho, A. M., Small, D., Wiggins, S., Ide, K., 2003. Computation of Stable and Unstable Manifolds of Hyperbolic Trajectories in Two-Dimensional, Aperiodically Time-Dependent Vectors Fields. *Physica D* 182, 188-222.
- [24] Mancho, A. M., Small, D., Wiggins, S., Ide, K., 2006. A comparison of methods for interpolating chaotic flows from discrete velocity data. *Computers and Fluids* 35, 416-428.
- [25] W.H. Press, S.A. Teukolsky, W.T. Vetterling, B.P. Flannery, *Numerical Recipes in Fortran 77, The Art of Scientific Computing*, 2nd ed., Cambridge University Press, Cambridge, 1999.
- [26] Dritschel, D.G., Contour dynamics and contour surgery: numerical algorithms for extended, high-resolution modelling of vortex dynamics in two-dimensional, inviscid, incompressible flows, *Comput. Phys. Rep.* 10 (1989) 77146.
- [27] Branicki, M, Mancho, A. M., Wiggins, S. A Lagrangian description of transport associated with a Front-Eddy interaction: application to data from the North-Western Mediterranean Sea. Preprint submitted for publication.

- [28] D. B. Chelton, M. G. Schlax, R. M. Samelson, and R. A. de Szoeke, Global observations of large oceanic eddies, *Geophysical Research Letters* 34 (2007), L15606.
- [29] Haller G, An objective definition of a vortex, *Journal of Fluid Mechanics* 525, 1-26 (2005).

### Figure captions

Figure 1

Solutions (6) for different initial conditions  $x^*$ . a) Solutions in positive times  $t > 0$ . b) Solutions in positive and negative times.

Figure 2

a) Function  $M(x^*)_{t=0,\tau}$  evaluated over the solutions (6). Dashed line  $\tau = 3$ , solid line  $\tau = 4$ . b) Position of the  $x^*$ -coordinate at the minimum of the function  $M_{t=0,\tau}$  as a function of  $\tau$ . The horizontal dashed line marks the position of the DT.

Figure 3

Position of the  $x^*$ -coordinate at the minimum of the function  $M_{t=0,\tau}$  as a function of  $\tau$ . The function  $M_{t=0,\tau}$  is considered for solutions in expression (8). The horizontal dashed line marks the position of the DHT.

Figure 4

Contour plot of the function  $M_{t=0,\tau=2}(\mathbf{x})$  in the open set  $\mathcal{D} = (-0.2, 0.2) \times (-0.2, 0.2)$ . The minimum corresponds to the black tone.

Figure 5

Contour plot of the function  $M$  in the open set  $\mathbf{x} \in (-0.2, 0.2) \times (-0.2, 0.2)$ . a)  $M_{t=0,\tau=5}(\mathbf{x})$ ; b)  $M_{t=0,\tau=10}(\mathbf{x})$ ; c)  $M_{t=0,\tau=50}(\mathbf{x})$ .

Figure 6

a)  $x$ -coordinate versus time for the DHT (thick solid line) and those trajectories integrated with initial conditions at the global minima of Figs. 5a) (solid line) and b) (dashed line); b)  $x$ -coordinate versus time for the DHT (thick solid line), a trajectory integrated with initial condition at the global minimum of Fig. 5c) (solid line) and a trajectory integrated at a non-global but relative minimum of the same figure (dashed line).

Figure 7

Evolution of the coordinates of the global minimum of  $M$  versus  $\tau$ . a) The  $x$  coordinate; b) the  $y$  coordinate. These plots show the convergence to the DHT whose position is marked with a dashed horizontal line.

Figure 8

A  $\delta$ -grid in  $\mathbb{R}^2$ . The centre or interior point is marked with the white dot.

Figure 9

A schematic projection onto the  $\mathbb{R}^2$  plane of a possible trajectory from  $-\tau$  to  $\tau$  with  $L$  points.

Figure 10

a) Representation of both the distinguished hyperbolic trajectory (11) and its approach obtained with the proposed numerical algorithm for  $\varepsilon = 0.1$ ; b) distance between the exact and the numerical approach.

Figure 11

Representation of the maximum  $\tau$  required to approach the DT within accuracy  $\delta = 10^{-6}$  versus time.

Figure 12

Contour plot of the function  $M$  in the open set  $\mathbf{x} \in (-1.2, -0.8) \times (-0.2, 0.2]$ .

a)  $M_{t=0, \tau=10}(\mathbf{x})$ ; b)  $M_{t=0, \tau=300}(\mathbf{x})$ .

Figure 13

Evolution of the coordinates of the global minimum of  $M$  versus  $\tau$  at  $t_0 = 0$ . a) The  $x$  coordinate; b) the  $y$  coordinate. These plots show the convergence of the minima to the coordinates of the DET whose position is marked with a continuous horizontal line.

Figure 14

a) Dotted line represents the exact non hyperbolic distinguished trajectory and the solid line stands for the numerically computed limit coordinates; b) distance between the exact non hyperbolic trajectory (20) and the limit coordinates.

Figure 15

a)  $x$ -coordinate versus time for the DET (solid line) and the trajectory integrated taking as initial data the limit coordinates located at time  $t_0 = 0$  (dashed line); b) time evolution of the differences between these trajectories.

Figure 16

a) Dashed line represents the exact distinguished hyperbolic trajectory of the rotating Duffing equation and the solid line stands for the numerically computed one; b) distance between the exact and the numerical distinguished hyperbolic trajectory.

Figure 17

Contour plot of the streamfunction produced by the quasigeostrophic model at day 300.

Figure 18

Distinguished hyperbolic trajectories in the Northern gyre of the quasigeostrophic model reported in [12]. a) Evolution of the  $x$  and  $y$  coordinates in the time interval  $[5, 338]$ ; b) evolution of the  $x$  and  $y$  coordinates in the time interval  $[450, 880]$

Figure 19

a) Solid line represents the distinguished hyperbolic trajectory depicted in Fig. 18a) and circles stands for the numerically computed limit coordinates; b) distance between the trajectories represented in a).

Figure 20

Circles stand for the  $x$  component of the limit coordinates in the time range where they approach a DT. The solid line represents a trajectory integrated with a 5th order Runge-Kutta method passing through limit coordinates at day 285. The dashed line is a trajectory integrated from the same condition plus a small perturbation.

Figure 21



a)  $x$  component of the minimum of  $M$  versus  $\tau$  at day 330; b)  $y$  component of the minimum of  $M$  versus  $\tau$  at the same day.

Figure 22

a) Circles stand for the  $x$  component of the limit coordinates versus time and the solid lines stand for different trajectories; b) the same as a) but for the  $y$  component.

Figure 23

a) Solid line represents the distinguished hyperbolic trajectory depicted in Fig. 18b) and circles stand for the numerically computed limit coordinates; b) distance between the trajectories represented in a).

Figure 24

a) Contour plot of  $M_{t=370, \tau=150}$ , the elliptic minimum is in the dark area almost at the centre; b) contour plot of  $M_{t=370, \tau=250}$ .

Figure 25

a)  $x$  component of the minimum of  $M$  versus  $\tau$  at day 370; b)  $y$  component of the minimum of  $M$  versus  $\tau$  at the same day.

### Table captions

Table 1

Relative errors in several ellipse lengths, computed with a linear interpolation over  $L$  points on the curve.

Table 2

Relative errors in several ellipse lengths, computed with Dritschel interpolation over  $L$  points on the curve.

$L$	Linear interpolation					
	Ratio between axes					
	1	2	5	10	100	1000
10	8.16	8.80	9.48	9.73	9.99	10.00
$10^2$	2.63	3.36	3.86	3.99	4.05	4.05
$10^3$	0.83	1.08	1.24	1.29	1.31	1.31
$10^4$	0.26	0.34	0.39	0.41	0.41	0.41
$10^5$	$8.34 \times 10^{-2}$	0.11	0.12	0.13	0.13	0.13
$10^6$	$2.64 \times 10^{-2}$	$3.42 \times 10^{-2}$	$3.94 \times 10^{-2}$	$4.08 \times 10^{-2}$	$4.14 \times 10^{-2}$	$4.14 \times 10^{-2}$
$10^7$	$8.34 \times 10^{-3}$	$1.08 \times 10^{-2}$	$1.25 \times 10^{-2}$	$1.29 \times 10^{-2}$	$1.31 \times 10^{-2}$	$1.31 \times 10^{-2}$
$10^8$	$2.64 \times 10^{-3}$	$3.42 \times 10^{-3}$	$3.95 \times 10^{-3}$	$4.08 \times 10^{-3}$	$4.14 \times 10^{-3}$	$4.14 \times 10^{-3}$
$10^9$	$8.34 \times 10^{-4}$	$1.08 \times 10^{-3}$	$1.25 \times 10^{-3}$	$1.29 \times 10^{-3}$	$1.31 \times 10^{-3}$	$1.31 \times 10^{-3}$

Table 1:

$L$	Dritschel interpolation					
	Ratio between axes					
	1	2	5	10	100	1000
10	0.99	0.67	0.33	0.25	0.26	0.27
$10^2$	$3.49 \times 10^{-2}$	$1.37 \times 10^{-2}$	$4.47 \times 10^{-3}$	$2.81 \times 10^{-3}$	$2.08 \times 10^{-3}$	$2.61 \times 10^{-3}$
$10^3$	$1.11 \times 10^{-3}$	$3.83 \times 10^{-4}$	$9.20 \times 10^{-5}$	$4.43 \times 10^{-5}$	$2.23 \times 10^{-5}$	$1.98 \times 10^{-5}$
$10^4$	$3.53 \times 10^{-5}$	$1.17 \times 10^{-5}$	$4.44 \times 10^{-6}$	$5.23 \times 10^{-6}$	$2.80 \times 10^{-7}$	$7.01 \times 10^{-7}$
$10^5$	$1.12 \times 10^{-6}$	$3.64 \times 10^{-7}$	$2.17 \times 10^{-6}$	$4.48 \times 10^{-6}$	$5.45 \times 10^{-8}$	$9.20 \times 10^{-7}$
$10^6$	$3.51 \times 10^{-8}$	$1.14 \times 10^{-8}$	$2.10 \times 10^{-6}$	$4.46 \times 10^{-6}$	$5.222 \times 10^{-8}$	$9.22 \times 10^{-7}$
$10^7$	$1.11 \times 10^{-9}$	$3.68 \times 10^{-10}$	$2.10 \times 10^{-6}$	$4.46 \times 10^{-6}$	$5.21 \times 10^{-8}$	$9.22 \times 10^{-7}$
$10^8$	$2.18 \times 10^{-11}$	$1.30 \times 10^{-11}$	$2.10 \times 10^{-6}$	$4.46 \times 10^{-6}$	$5.22 \times 10^{-8}$	$9.22 \times 10^{-7}$
$10^9$	$3.72 \times 10^{-10}$	$3.37 \times 10^{-10}$	$2.10 \times 10^{-6}$	$4.46 \times 10^{-6}$	$5.22 \times 10^{-8}$	$9.25 \times 10^{-7}$

Table 2:

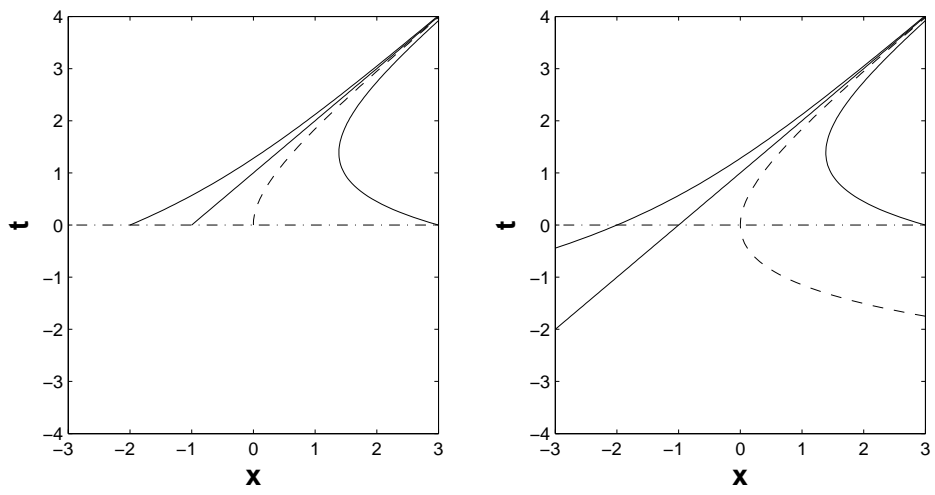
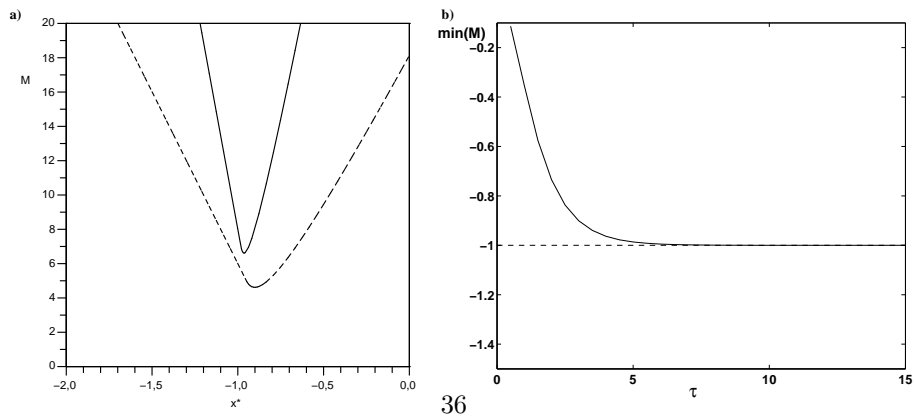


Figure 1:  
35



36

Figure 2:

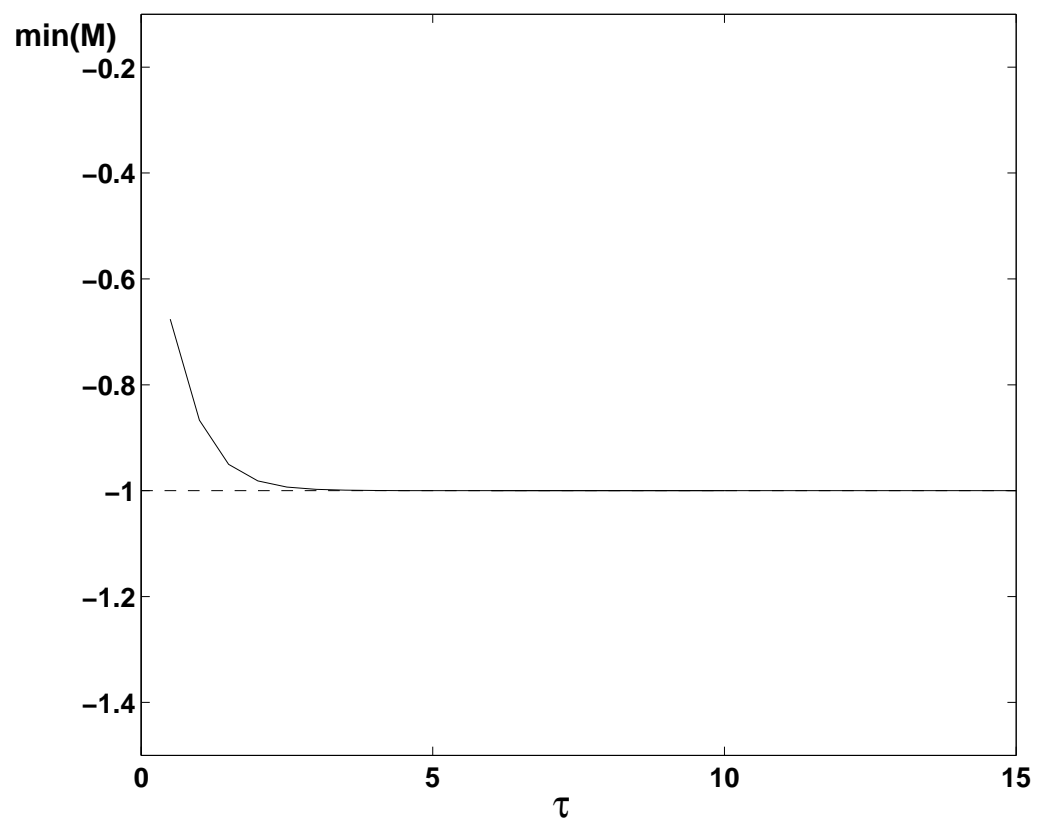


Figure 3:

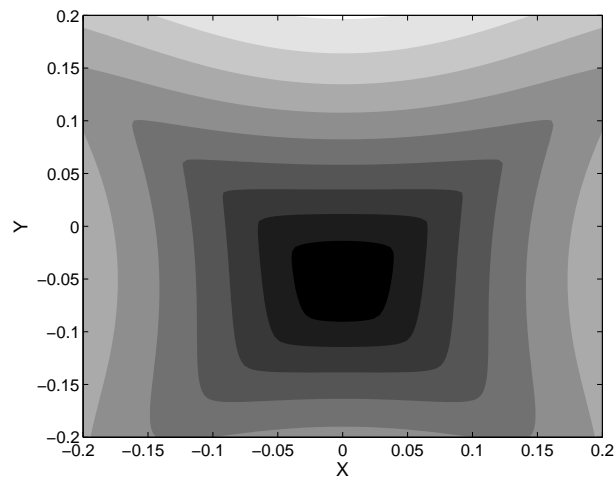


Figure 4:

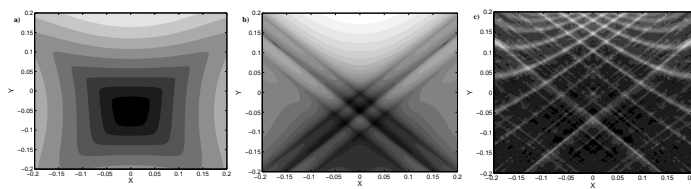


Figure 5:

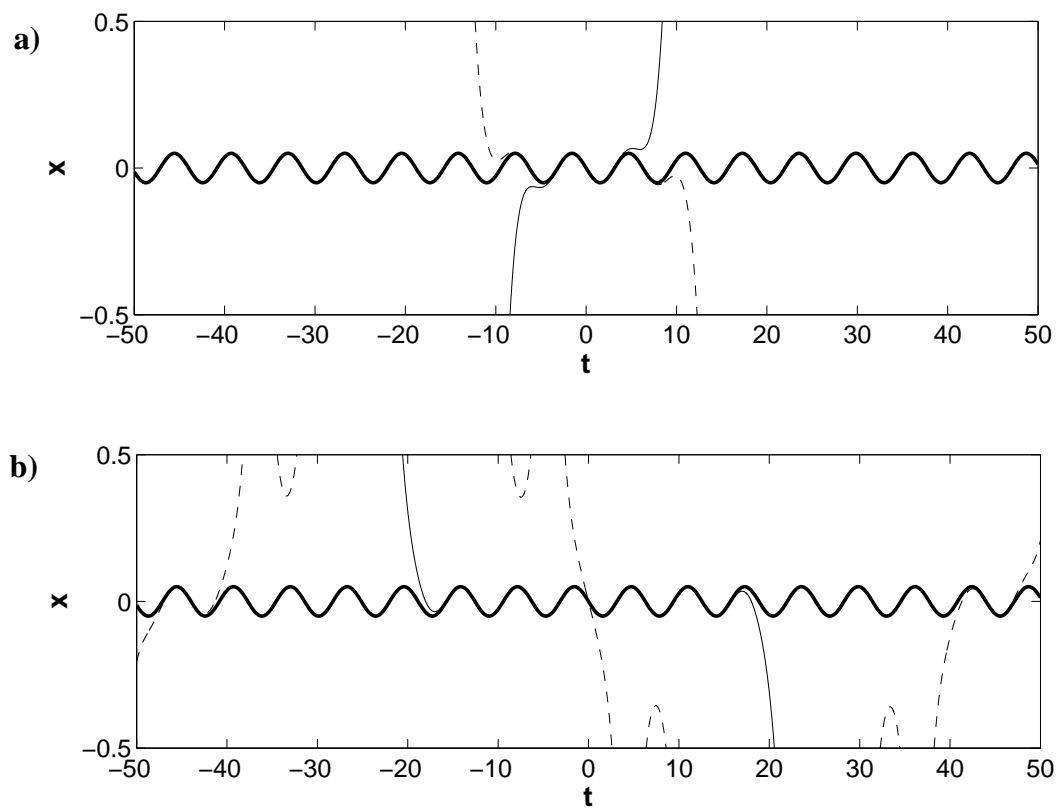


Figure 6:  
40



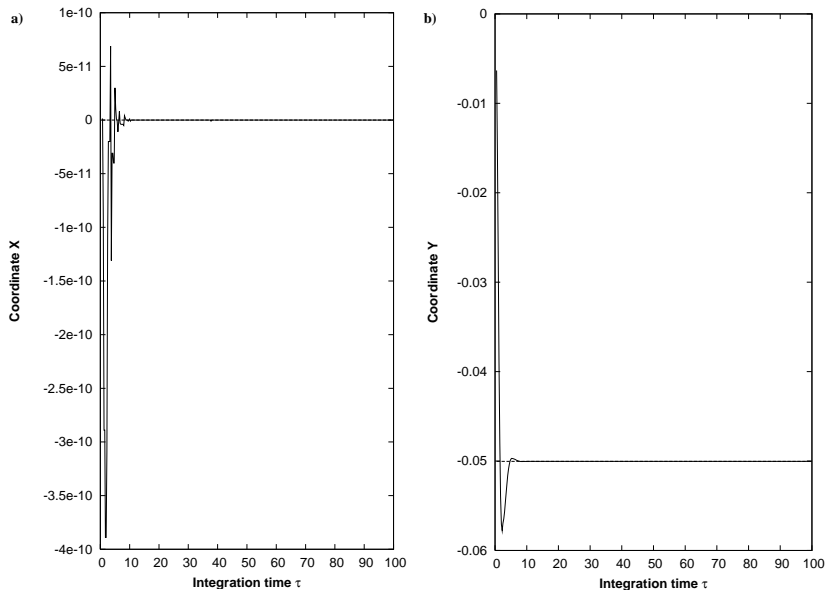


Figure 7:  
41

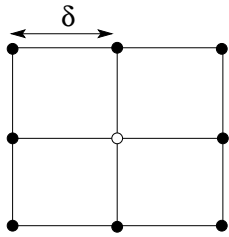


Figure 8:

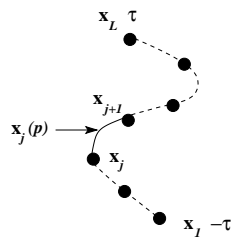


Figure 9:

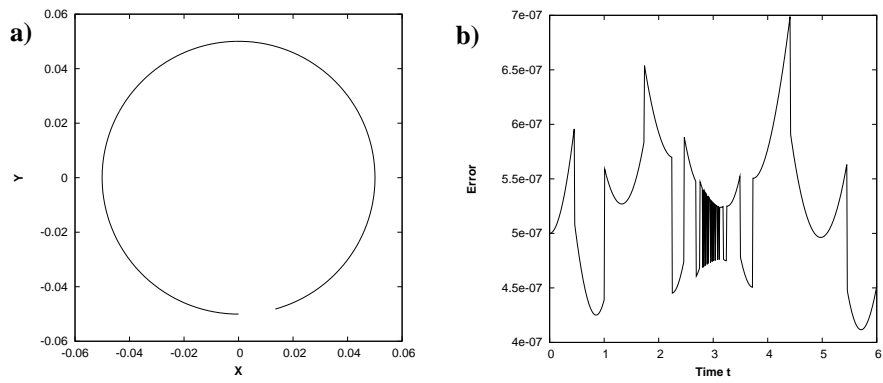


Figure 10:

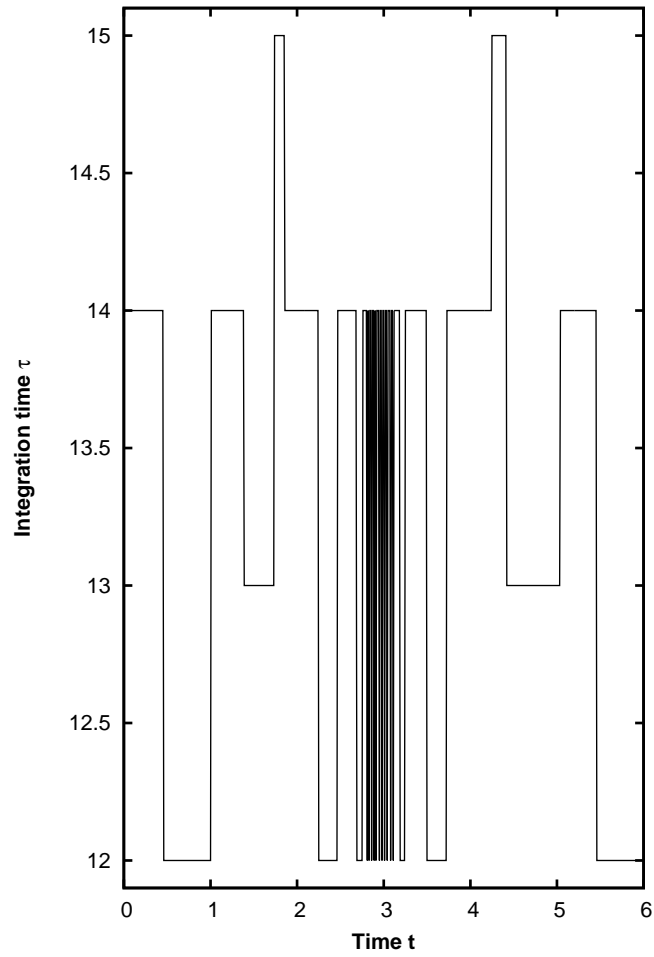


Figure 11:

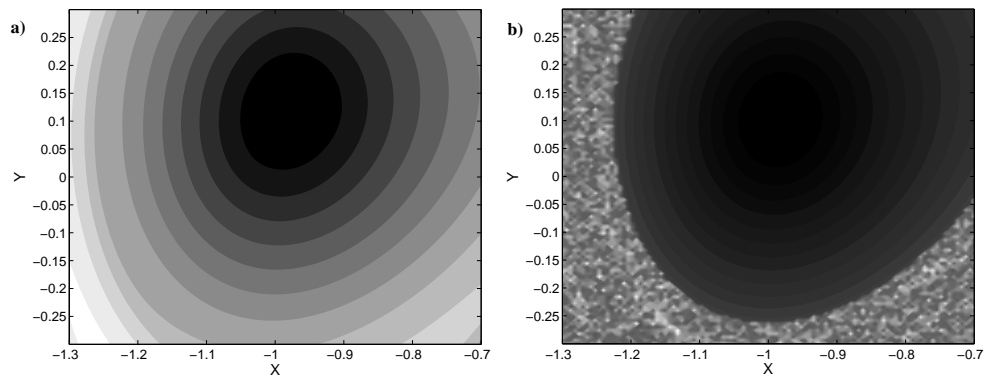


Figure 12:  
46

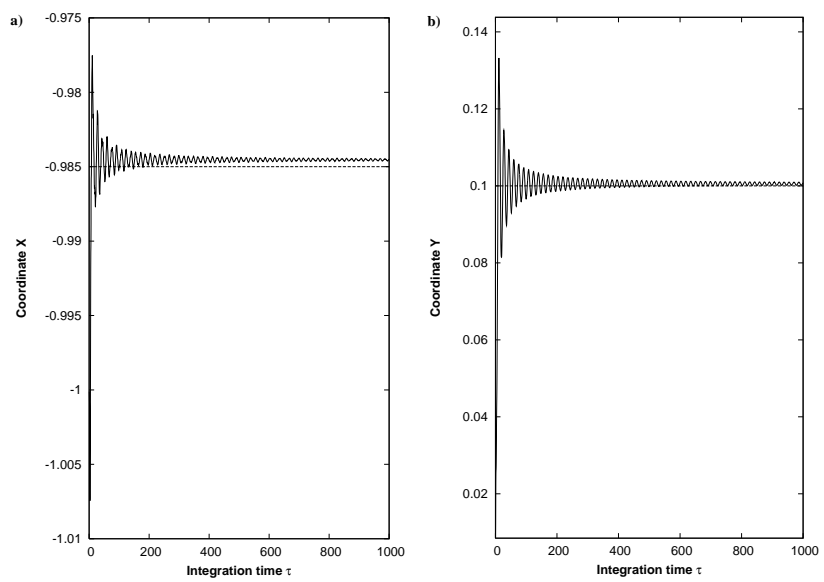


Figure 13:

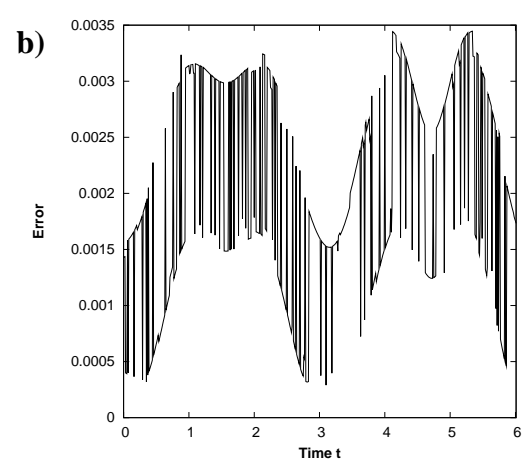
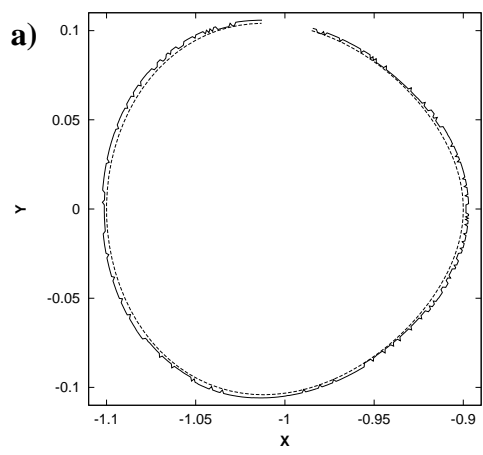


Figure 14:  
48



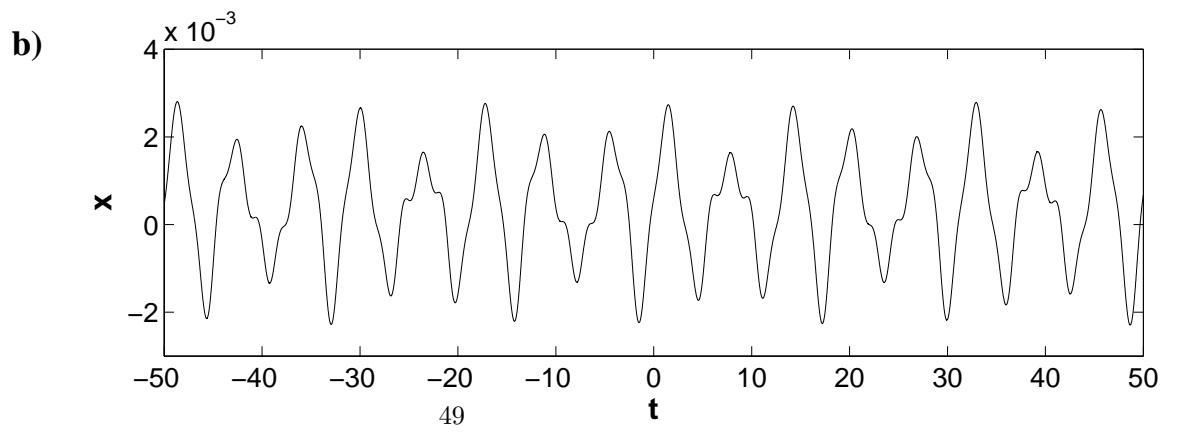
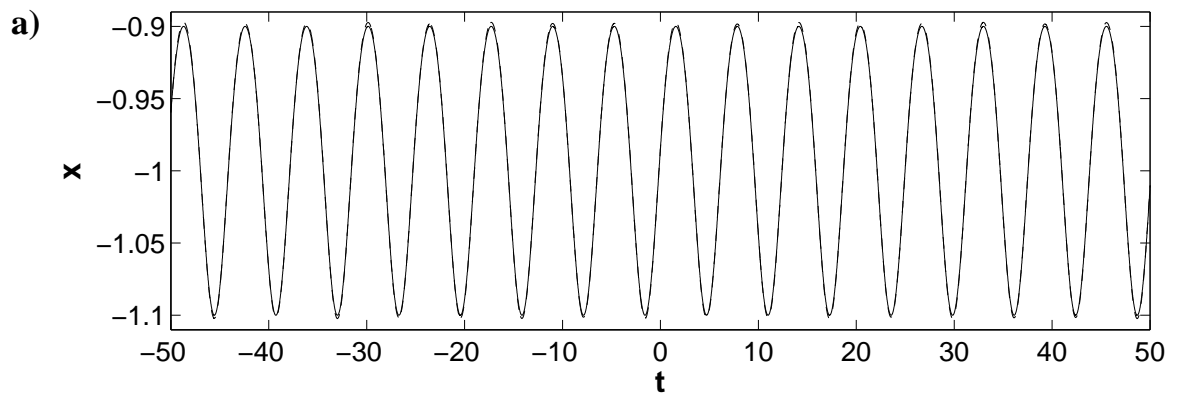


Figure 15:

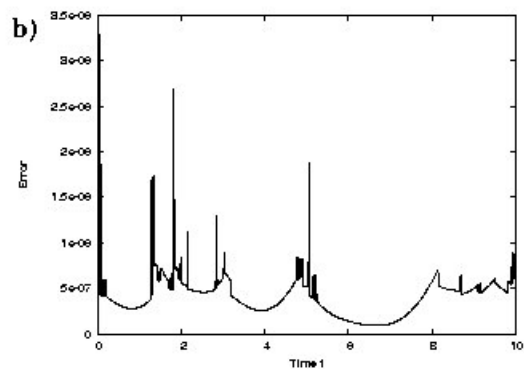
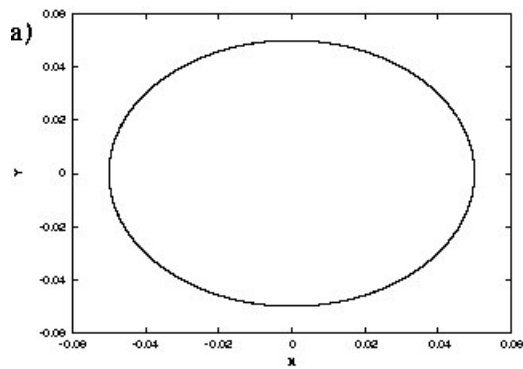


Figure 16:

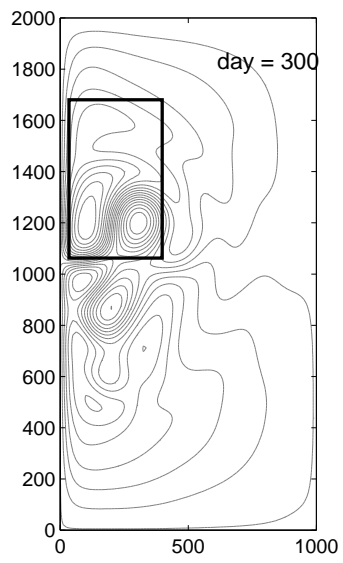


Figure 17:

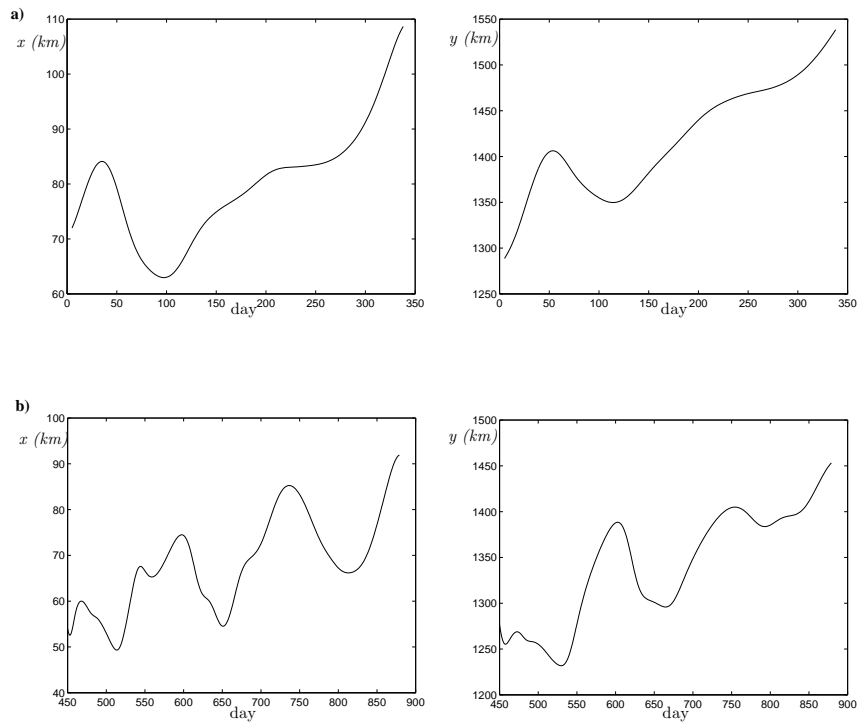


Figure 18:

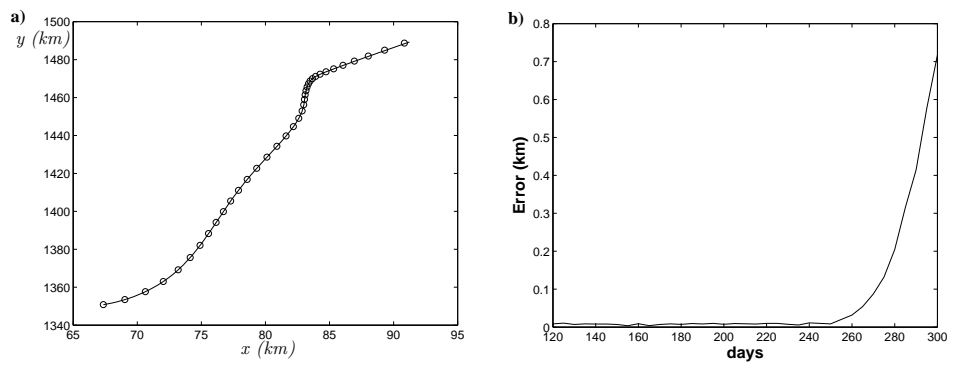


Figure 19:

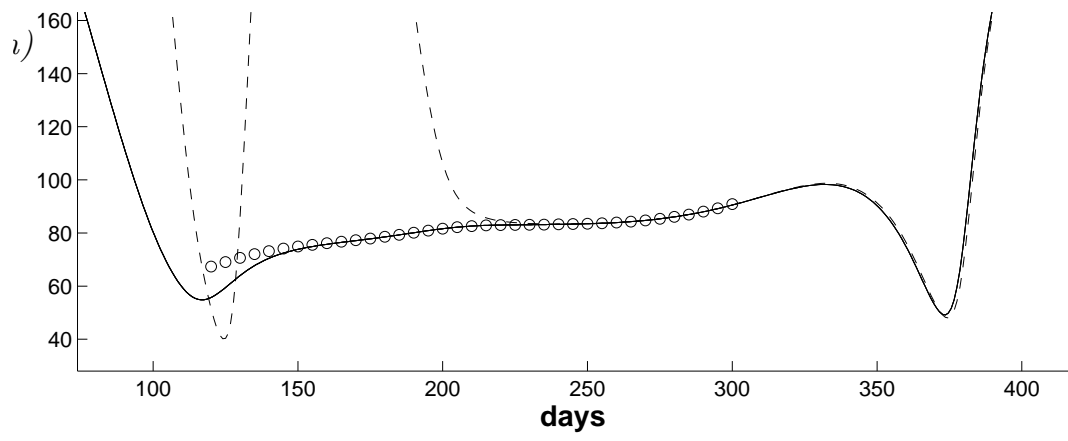


Figure 20:

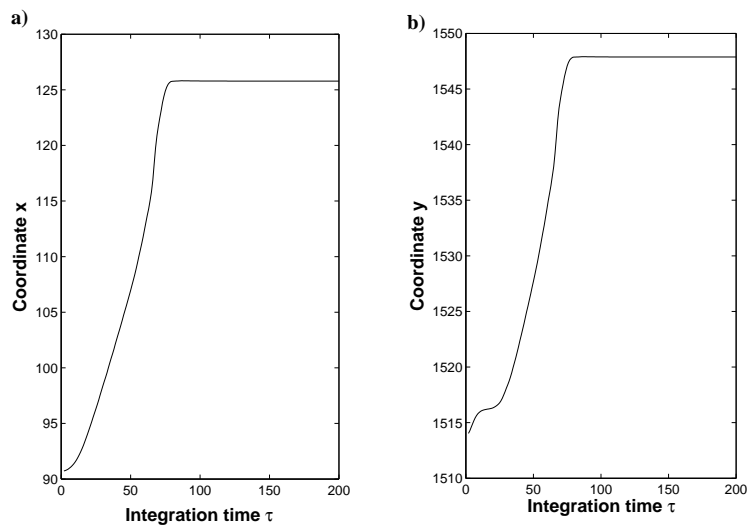


Figure 21:

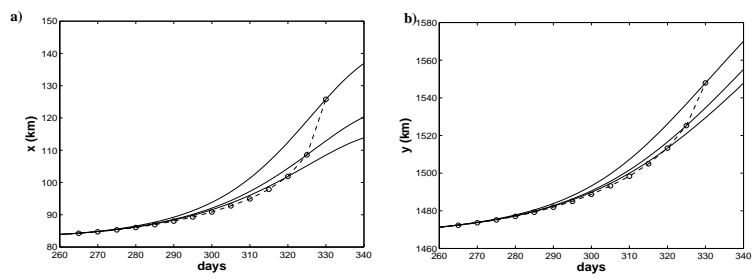


Figure 22:



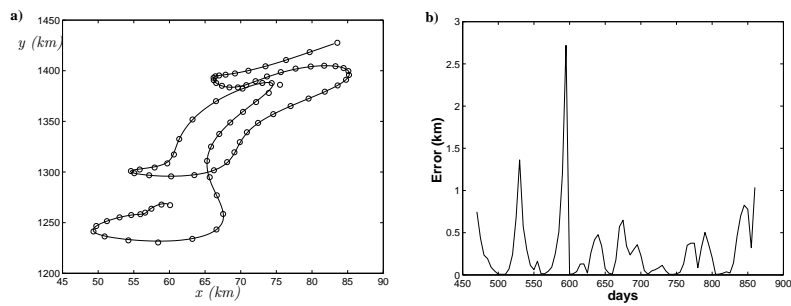


Figure 23:

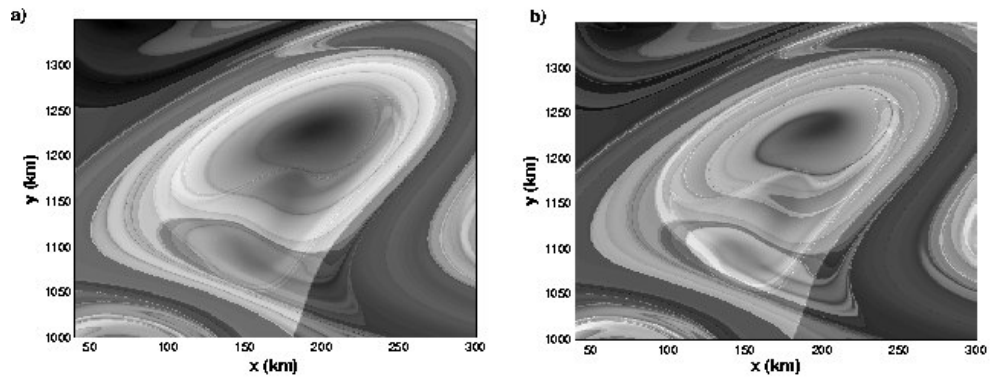


Figure 24:

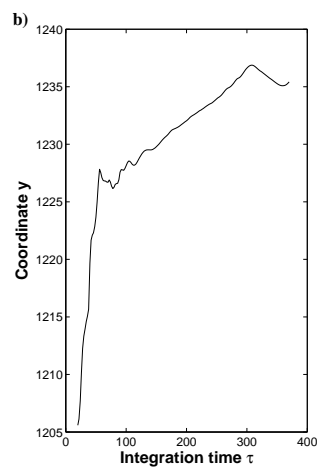
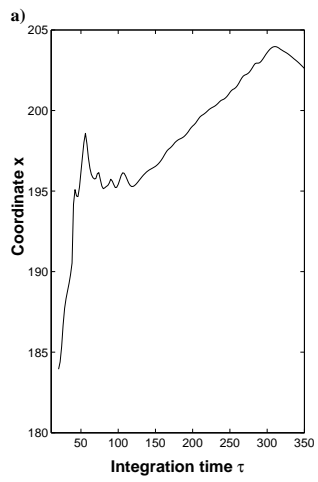


Figure 25:  
59